TOKAMAK FORMATION VIA LOCALIZED HELICITY INJECTION USING TANGENTIAL BOUNDARY FLOWS

P.L. GARCIA-MARTINEZ, R. FARENGO, H.E. FERRARI
CONICET-CNEA & Instituto Balseiro, Centro Atomico Bariloche
San Carlos de Bariloche, RN, Argentina
Email: pablogm@cab.cnea.gov.ar

Abstract

Non-solenoidal plasma initiation is a critical capability for future tokamak reactors. This work investigates the feasibility of tokamak formation via localized helicity injection (LHI) through time-dependent, three-dimensional magnetohydrodynamic (MHD) simulations. The study models the TCABR upgrade, a conventional aspect-ratio tokamak, and implements the helicity injection mechanism via localized tangential flows at the chamber's end-wall. Our simulations successfully reproduce the formation of a tokamak-like state, characterized by closed poloidal flux contours and a sustained toroidal current, following a strong magnetic relaxation event. Three cases with varying vertical field strengths and a fixed flow amplitude are analyzed. The results reveal that the efficacy of the startup is not monotonic with the helicity injection rate. An intermediate driving strength yields the most favorable outcome, enabling effective current redistribution into the plasma core via intermittent relaxation and resulting in a higher saturated toroidal current. In contrast, a configuration with the strongest injection becomes dominated by a edge-localized current filament, leading to higher dissipation and lower overall toroidal current. We conclude that LHI can be effectively modeled using boundary flows, to study solenoid-free startup in conventional aspect-ratio tokamaks. The success of this startup scheme depends critically on optimizing the helicity injection rate relative to the confining vertical field to maximize the current multiplication factor.

1. INTRODUCTION

Most contemporary tokamak and spherical tokamak experiments supply the initial current drive needed for plasma formation and ramp-up of the plasma current using induction from the central solenoid. A non-solenoidal plasma initiation scheme would allow to save inductive volt-second during startup that can then be utilized to extend the long-pulse, high-current operational regime. For this reason, solenoid-free startup methods are considered a crucial component of many present experiments, as well as future burning plasma devices.

A variety of solenoid-free startup methods have been developed, exploiting techniques like helicity injection, radiofrequency (RF) waves, or induction from poloidal field (PF) coils [1]. Among helicity injection approaches, localized helicity injection (LHI) employs high-power electron current injectors near the plasma edge to produce thin current filaments that wrap around the plasma forming a helical structure. At low injector currents, these filaments follow the nearly unperturbed vacuum magnetic field. As the injected current increases, the configuration becomes unstable and relaxes to a tokamak-like state [2]. Previous experiments have demonstrated the feasibility of this mechanism to form and sustain tokamak plasmas with conventional aspect ratio [3].

The underlying physics of this process is described by the theoretical framework of magnetic relaxation. In its basic form, this principle states that an unstable, turbulent plasma will evolve towards a minimum energy state while conserving its global magnetic helicity [4]. However, this constrained minimization analysis cannot be directly applied to the present situation, where the process is intrinsically dynamic, with helicity being continuously injected and dissipated. The dynamics of magnetic relaxation in complex geometries can be studied using magnetohydrodynamic (MHD) simulations, though this is challenging due to the inherently time-dependent and three-dimensional nature of the problem.

Previous work has used MHD simulations to study flux-rope evolution during the initiation of spherical tokamaks [5]. A key limitation of the standard MHD model is that it does not include charge separation; consequently, an electric potential difference across magnetic field lines can not be modeled. To overcome this, the effect of the injector in such framework was represented as a localized volumetric current source [5].

In this work, we present time-dependent, three-dimensional MHD simulations of the formation and sustainment of tokamak-like plasmas via LHI. Our study has two key differences from previous works. First, we consider the geometry of the TCABR upgrade, a conventional aspect-ratio tokamak [6]. A primary motivation for this effort is to contribute to the design of a solenoid-free startup system for this device. Second, our model implements the helicity injection mechanism through boundary flows, a genuine boundary condition that has been used previously to study relaxation dynamics [7]. Our results demonstrate the feasibility of using LHI to initiate a tokamak-like

configuration in the TCABR upgrade geometry. They also indicate that an adequate balance between the helicity injection rate and the vertical magnetic field strength is essential to maximize toroidal current driving.

2. MODEL DESCRIPTION

2.1. Governing equations and numerical method

Simulations in this study are performed with VAC (Versatile Advection Code) [8], a numerical code originally developed for the astrophysics community, in which the finite-volume method for solving the compressible hydrodynamic and MHD equations is implemented. In particular, this code can be used to solve the isothermal resistive MHD model, which is the one employed in this work. The isothermal-MHD equations are non-dimensionalized using a length scale L, a density scale ρ_0 and a magnetic field scale B_0. With these quantities we can define the Alfvèn velocity scale $c_A = B_0/\sqrt{\mu_0\rho_0}$, the Alfvèn time $\tau_A = L/c_A$, and the current scale $J_0 = B_0/L\mu_0$.
The resulting dimensionless equations are

$$\frac{\partial \rho}{\partial t} + \nabla \cdot (\rho \mathbf{u}) = 0 \tag{1}$$

$$\frac{\partial \mathbf{u}}{\partial t} + \mathbf{u} \cdot \nabla \mathbf{u} + \beta \frac{\nabla p}{\rho} = \frac{\mathbf{J} \times \mathbf{B}}{\rho} + \tilde{\nu} \nabla \cdot \Pi \tag{2}$$

$$\frac{\partial \mathbf{B}}{\partial t} + \nabla \times \mathbf{E} = 0, \tag{3}$$

where, $\mathbf{J} = \nabla \times \mathbf{B}$, $\mathbf{E} = -\mathbf{u} \times \mathbf{B} + \tilde{\eta}\mathbf{J}$, $\Pi = (\nabla \mathbf{u} + \nabla \mathbf{u}^{\mathrm{T}}) - \frac{2}{3}(\nabla \cdot \mathbf{u})$, $p = c_s^2 \rho$ (isothermal assumption), where c_s is the sound speed, and $\beta = \mu_0 p_0 / B_0^2 = c_s^2/c_A^2$. The parameter $\tilde{\nu} = \nu/(Lc_A)$ is the dimensionless kinematic viscosity and $\tilde{\eta} = \eta/(\mu_0 L c_A)$ is the dimensionless resistivity, both considered spatially uniform. In this work we use $\beta = 0$ (uniform density), $P_m = \tilde{\nu}/\tilde{\eta} = 1$ (magnetic Prandtl) and $\tilde{\eta} = 10^{-4}$. For simplicity, the length scale is $L = 1$ m and $B_0 = 1$ T (toroidal field at the geometric axis), thus, non-dimensional lengths and magnetic fields coincide numerically with SI units. Time is expressed in Alfvèn times, which gives $t_A \approx 0.2$ μs, for deuterium at a number density $\sim 10^{-19}$ m^{-3}.

2.2. Geometry, boundary conditions and run parameters

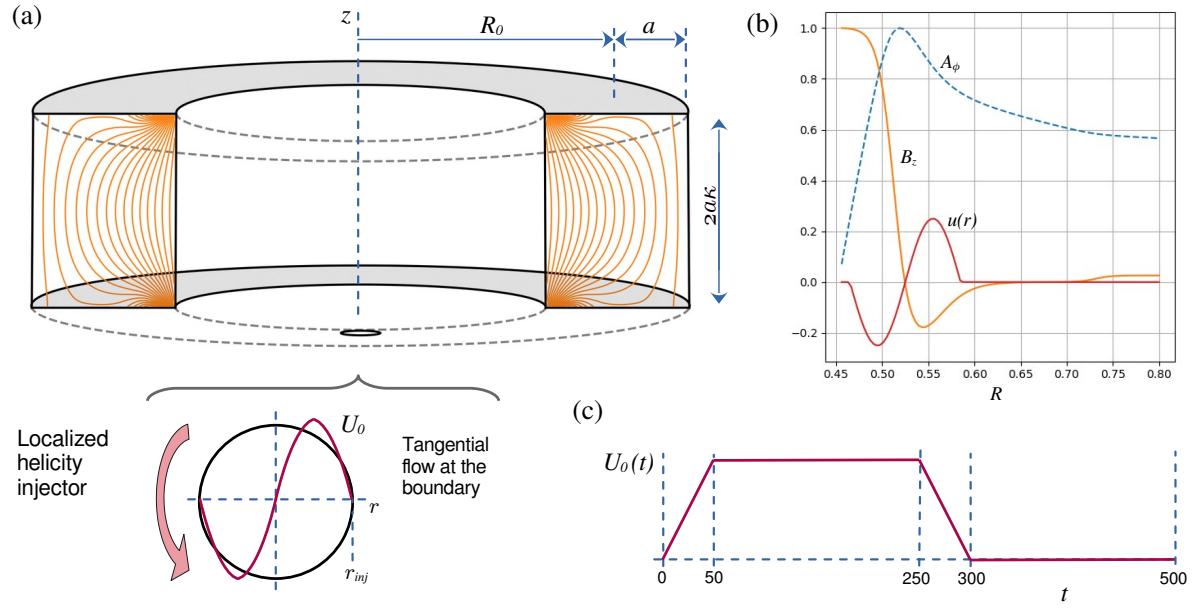

FIG. 1. (a) Geometry of the flux conserver, vertical magnetization (initial magnetic flux contours in orange) and detail of the localized boundary flow imposed at the bottom end. (b) Profiles of the quantities involved in helicity injection. (c) Time dependence of the amplitude of the imposed driving flow at the boundary.

To model TCABR we consider a toroidal flux conserver with rectangular cross section as the domain for the calculation. The major and minor radii are $R_0 = 0.628$ m and $a = 0.172$ m respectively and the elongation κ

is 1.45, as indicated in Fig. 1 (a). The boundary conditions for the magnetic field in the flux conserving walls are (i) imposed normal field $\mathbf{B}\cdot\mathbf{n}$ and (ii) zero order extrapolation of tangential field $\nabla(\mathbf{B}\times\mathbf{n})\cdot\mathbf{n}=0$. In the lateral walls the normal (i.e. radial) field is zero. In the bottom and top ends, the imposed normal field (B_z) has the profile shown in Fig. 1 (b). The maximum value B_{z0} of the vertical magnetization is located at the inner limit ($R=R_0-a$) and has negative values in the band $0.525<R<0.625$, for helicity injection purposes as explained below.

The boundary condition for the normal velocity is zero everywhere. Tangential velocity is zero everywhere excepting at the injector, which is modeled as a disc with radius $r_{inj}=0.06$ in the base, centered at $R_{inj}=0.525$ and toroidal position $\phi=0$, as indicated in Fig. 1. Within this disc the tangential velocity is a rotation with sinusoidal profile $u(r)$, where r is the distance to the center of the disc and u points in the azimuthal direction within the disc.

The governing equations are solved in a regular grid with $(55\times65\times75)$ volumes in cylindrical coordinates (R,ϕ,z) during 500 Alfvèn times. The initial condition is the vacuum magnetic field given by the vertical magnetization B_z described before, plus the toroidal field B_0R_0/R produced by the central solenoid, and zero velocity everywhere. Three runs are analyzed in Sec. 3 with the same tangential flow amplitude $U_0=8$ and three different levels of vertical magnetization: (I) $B_{z0}=0.019$, (II) $B_{z0}=0.031$ and (III) $B_{z0}=0.032$, where B_{z0} is the maximum value of the magnetic field imposed at bottom and top ends of the chamber. Taking B_{z0} as representative of the vertical field and $B_0=1$ for the toroidal direction, these values produce field lines that approximately complete 6.5, 4 and 2 toroidal turns during the vertical transit. These values of the characteristic helical ratio H is only indicative, as the vacuum fields vary in R and z and are strongly distorted during intense MHD activity.

2.3. Helicity injection

Helicity is given by $K=\int_V\mathbf{A}\cdot\mathbf{B}\,\mathrm{d}^3x$, where $\mathbf{A}$ is the magnetic vector potential. The evolution of helicity is given by [9],

$$\frac{\mathrm{d}K}{\mathrm{d}t}=-2\int_V\eta\mathbf{J}\cdot\mathbf{B}\,\mathrm{d}V-2\int_S\Phi\mathbf{B}\cdot\mathbf{n}\,\mathrm{d}S-2\int_S[(\mathbf{A}\cdot\mathbf{B})(\mathbf{u}\cdot\mathbf{n})-(\mathbf{A}\cdot\mathbf{u})(\mathbf{B}\cdot\mathbf{n})]\,\mathrm{d}S, \tag{4}$$

where the first term describes the resistive dissipation of helicity, the second gives the "dc" helicity injection produced by an applied electrostatic potential Φ (zero in the MHD framework), the third term involves flow across the boundary (also zero in our case) and finally, the term $(\mathbf{A}\cdot\mathbf{u})(\mathbf{B}\cdot\mathbf{n})$ gives the helicity injection produced by motions of the footpoints of the penetrating magnetic field. This is the relevant term which quantifies the helicity injected by the boundary condition imposed. From the profiles shown in Fig. 1 (b), it is clear that this term in non-zero, in fact, it is negative for positive U_0 (for the adopted direction). Note that the center of the disc was intentionally put in the zero crossing of B_z, so the two relevant terms, $\mathbf{A}\cdot\mathbf{u}$ and $\mathbf{B}\cdot\mathbf{n}$, simultaneously change their sign.

Relaxed states, i.e. minimum energy states for a given amount of helicity, have uniform λ defined as

$$\lambda=\frac{\mathbf{J}\cdot\mathbf{B}}{B^2}. \tag{5}$$

In a driven configurations like the ones considered here, fully relaxed states are never attained. However, relaxation acts to redistribute the current and to flatten the λ gradient imposed by the helicity injector. Therefore, the spatial distribution of λ is a good indicator whether the configuration is close to a relaxed state (weak driving) or the current profile is dominated by the external driving (see Fig. 4 and the discussion therein for an example).

3. RESULTS

3.1. Current at the injector and toroidal current

By imposing a localized rotation at the point where the magnetic flux changes sign at the boundary currents must be produced by the twisting of field lines. The value of the net current through the injector driven by this boundary condition can be calculated by integrating J_z in the vicinity of the disc. In practice we integrated J_z throughout all the base. The resulting vertical current is plotted in Fig. 2 (a) for the three runs. As expected from the geometry of the boundary condition and Eq. 4 the net value is negative during the driving phase ($50<t<250$), but the sign was inverted in the plot for presentation purposes.

The distribution of J_z at the base in run (II) is shown at two times in Fig. 3 (a) and (b). The current is mainly localized around the injector disc, but there is a significant fraction that flows aligned with the vertical field at other toroidal positions. Several complex structures of pairs of co and counter current channels are formed. These

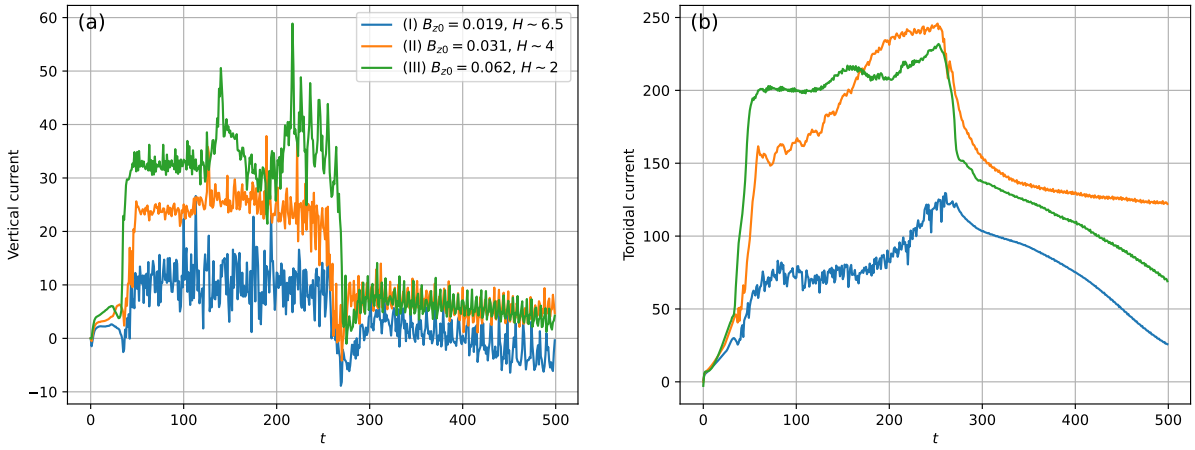

FIG. 2. Evolution of (a) the vertical current at the base (proxy for the injector current) and (b) the total toroidal current along the plasma for three different magnetization intensities. H is the helical ratio of a typical field line (toroidal turns during the vertical transit).

structures have a very rapid dynamics, which explains the level of fluctuations observed in the total vertical current shown in Fig. 2 (a). The distribution of J_z through the top of the chamber is also highly dynamical but is not localized as can be observed in Fig. 3 (c). The difference between the total vertical current through the top and bottom ends is typically below 9%.

The currents driven through the base flow along the field lines inducing a toroidal component. This process is approximately linear at the beginning ($t < 50$), as shown in Fig. 2 (b), until a relaxation event produces a significant toroidal current amplification. The current amplification level of this initial relaxation event is proportional to the helicity injection rate, which scales as the square of B_{z0} as can be deduced from the last term in eq. 4. However, the stronger the relaxation event the higher the dissipation which explains the low saturation level con case (III). Note that current after relaxation ($t \approx 80$) for case (II) is twice the current achieved in case (I), which is roughly the same ratio that the helicity injaction rate between these cases. But case (III) relaxes towards a toroidal current ≈ 200, only a fraction larger than case (II), which has four times less helicity injection rate. Moreover, during sustainment, there is a significant build up of additional toroidal current in cases (I) and (II), as a consequence of smaller intermittent relaxation events, but only a marginal increase in case (III).

3.2. Plasma initiation and sustainment phase

The relaxation event that suddenly increases the toroidal current also involves the formation of closed poloidal flux contours, as shown in Fig. 4 (a) and (d) for cases (I) and (III). These closed contours in ψ, the poloidal magnetic flux, result from the integration of B_z in the whole toroidal direction, so they represent an axisymmetric "tokamak-like" structure only in an averaged sense. Due to the high level of fluctuations during sustainment, these contours do not coincide with actual flux surfaces. The contour $\psi = 0$ divides open and closed contours. Closed

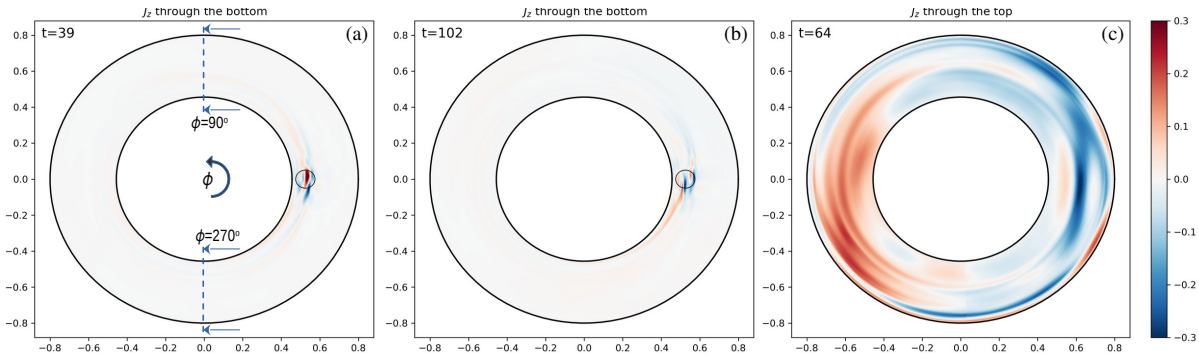

FIG. 3. Vertical current density distribution at (a-b) the base and at (c) the top for run (II) at different times. The injector disc is indicated with a circle at $\phi = 0$. Panel (a) shows the poloidal planes taken for figures 4, 5 and 6.

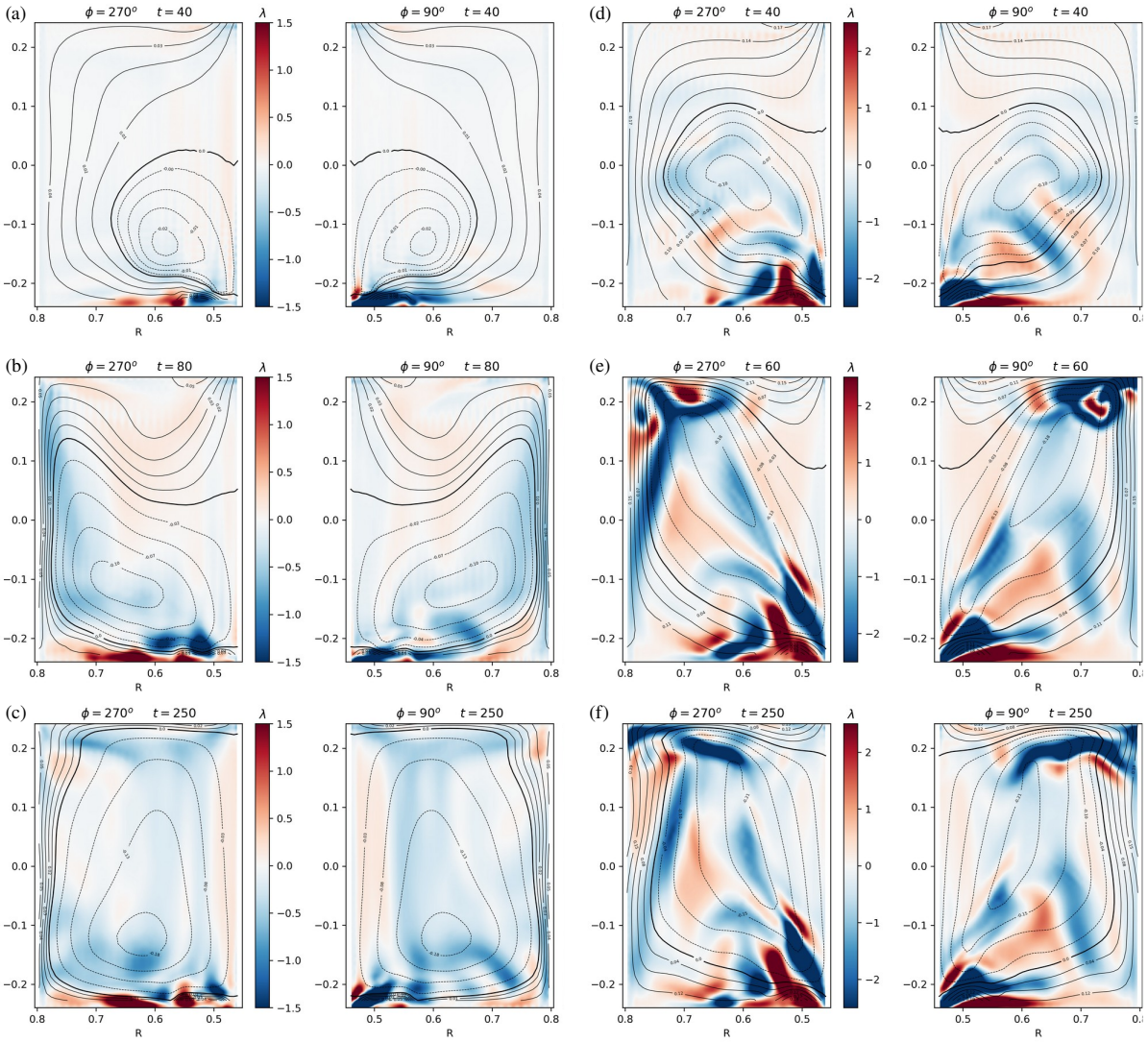

FIG. 4. Contours of poloidal magnetic flux and colormaps of λ in two poloidal planes ($\phi = \pi/2$ and $\phi = 3\pi/2$) at three times for (a-c) case (I) and (d-f) case (III).

contours have negative values indicating that toroidal current flows in the negative ϕ direction (anti parallel with respect to B_0).

Fig. 4 also displays colormaps of λ, taken at the two specific toroidal positions shown in Fig. 3 (a). Thus, these maps show the toroidal asymmetry of the fluctuation pattern. The panels on left side (a-c) correspond to case (I) that has the weaker driving. In this case, the closed contour region grows gradually during the sustainment phase until it expands to occupy almost all the cross section. Recall that this case has the lowest magnetization level, so the open flux region can be more easily compressed than in the other cases. During the relatively slow expansion of the plasmoid, relaxation acts to flatten the λ profile there. Intense λ gradients only persist in the region adjacent to the base, where current filaments from the injector are highly localized.

The panels (d-f) on the right of Fig. 4, shown an example of strongly driven configuration. In this case the plasmoid delimited by the $\psi = 0$ contour grows explosively towards the opposite corner of the poloidal plane, as can be inferred from the comparison of panels (d) and (e) which are separated by only 20 Alfvén times. The current filament settles in the outer-top corner and remains there, forming a diagonal negative current channel as the dominant structure during the sustainment phase. The λ distribution is highly inhomogeneous in the closed contour region indicating that the driving overcomes the natural tendency of the plasma to relax.

Case (II) has an intermediate level of helicity injection and shows a mixed behavior. In the first relaxation event, an explosive growth of the plasmoid similar to case (III) is observed, casing the current channel from the injector to concentrate in the outer-top corner of the poloidal plane. However, in this case, a series of smaller relaxation events in the early stage of the sustainment phase (see Fig. 2b at $90 \lesssim t \lesssim 120$) redistribute the current from the

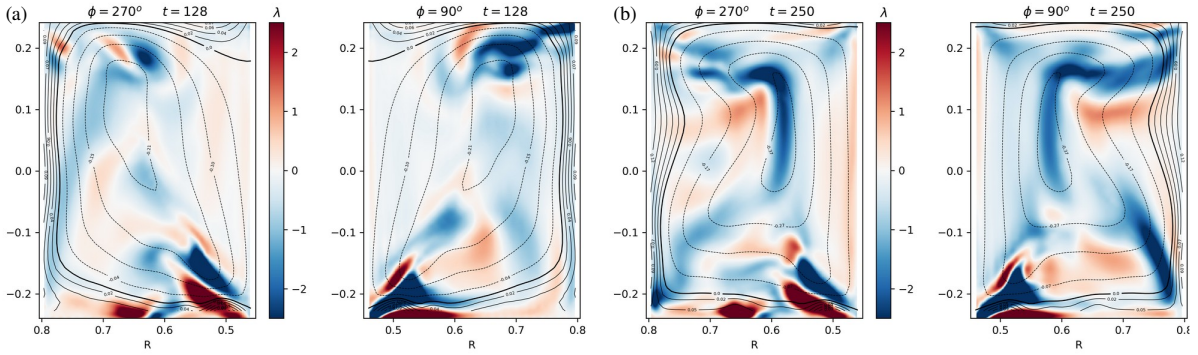

FIG. 5. Contours of poloidal magnetic flux and colormaps of λ in two poloidal planes ($\phi = \pi/2$ and $\phi = 3\pi/2$) at three times for case (II) (a) at $t = 128$ during sustainment and (b) at $t = 250$ when sustainment is gradually turned off.

injector towards the closed flux region, as can be observed in Fig. 5 (a). As a result, there is a build up of toroidal current during the second half of the sustainment phase, that reaches higher values than the more strongly driven case (III).

3.3. Decay phase

When the driving is turned off (this is done by decreasing U_0 to zero in the time interval $250 < t < 300$) the configuration tends to an axisymmetric tokamak state. A large scale fluctuation persists, which nonetheless produces a periodic bouncing of the main negative current channel and the closed flux contours. This fluctuation is observed as a positive flowing current density (λ in the plot) in high field side at $\phi = 90^\circ$ in Fig. 6 (b) and at $\phi = 270^\circ$ in Fig. 6 (c). In case (I), Fig. 6 (a), the bouncing is gentler and occurs in the vertical direction. There are also persistent high frequency fluctuations near the bottom and the injector that prevent the vertical current at the base from going exactly to zero (see Fig. 2a).

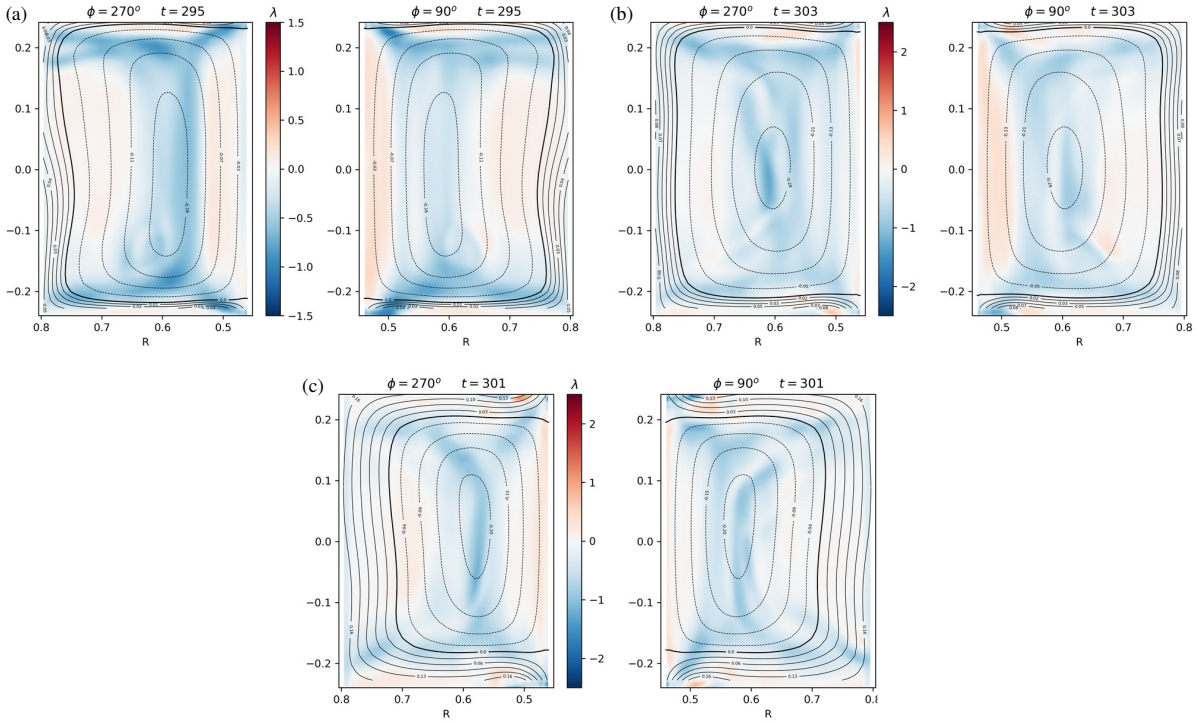

FIG. 6. Contours of poloidal magnetic flux and colormaps of λ in two poloidal planes ($\phi = \pi/2$ and $\phi = 3\pi/2$) during the decay phase for (a) case (I), (b) case (II) and (c) case (III).

The behavior of the toroidal current in the decay phase, $t > 300$, observed in Fig. 2 (b) is clarified by the comparison of the configurations at $t \approx 300$ shown in Fig. 6. Due to the lower helicity injection rate in cases (I) and (II), relaxation events were able to redistribute more current into the closed contour region, thus, more magnetic flux is trapped there when sustainment ceases. In addition, the magnetization is weaker in these cases, so the ratio closed to open flux is significantly larger: $\sim 0.16/0.04 \approx 4$ in case (I), $\sim 0.3/0.08 \approx 3.7$ in case (II) and $\sim 0.21/0.16 \approx 1.3$ in case (III).

Another interesting aspect of the decay phase is the decay rate of toroidal current (and poloidal flux) just after the sustainment flat-top ($250 < t < 300$). Cases (II) and (III) experience a very rapid drop due to the high current gradients present in strongly driven configurations. Case (I) instead, exhibits much slower decay, since the dynamics of relaxation was able to redistribute current at a rate similar to the current injection rate.

4. CONCLUSIONS

Time-dependent, three-dimensional magnetohydrodynamic (MHD) simulations have been performed to investigate the formation and sustainment of a tokamak-like plasma via localized helicity injection (LHI) in the geometry of the TCABR upgrade. Helicity injection was produced by tangential boundary flows applied on a small disc at the bottom boundary in a region with magnetic field lines going into and out of the chamber. The simulations successfully reproduce the formation of closed poloidal flux surfaces following a magnetic relaxation event, transitioning from purely open vacuum field lines to a confined plasma state. This demonstrates the fundamental feasibility of initiating a tokamak-like configuration in a conventional aspect-ratio tokamak using LHI modeled as a boundary flow condition.

Three cases with increasing level of vertical magnetization (B_{z0}) and the same amplitude of the boundary flow (U_0) were analyzed. The helicity injection rate is linear in U_0 but scales as the square of B_{z0}, so the relation between helicity injection and magnetization also increases. The key findings of the study of these cases are as follows:

- Case (I), low B_{z0}: Under weak driving, the system undergoes a gradual relaxation, leading to a well-distributed current profile and a slowly expanding plasmoid. In the run presented, the overall toroidal current remained modest presumably because the sustainment phase was too short for this case, which is the only one that did not show signs of current saturation.

- Case (II), intermediate B_{z0}: Here, the initial relaxation is significant, in terms of toroidal current amplification. Subsequent smaller relaxation events during the sustainment phase effectively redistribute current from the edge injector into the closed flux region. This results in a higher final toroidal current and a larger ratio of closed-to-open magnetic flux.

- Case (III), high B_{z0}: With strong driving, an explosive initial relaxation occurs, and the configuration becomes overly dominated by the injector. The current remains concentrated in a filament, preventing efficient current redistribution into the core and leading to high dissipation and a lower saturation current despite a higher injection rate.

These results highlight that the efficacy of the startup is critically dependent on achieving an adequate balance between the helicity injection rate and the vertical magnetic field strength. A good indicator of the efficacy of this process is the current amplification factor, i.e. the ratio of toroidal plasma current to the injector current. From the comparison between panels (a) and (b) in Fig. 2 at the end of the sustainment phase ($t \approx 250$), we see a current multiplication ~ 12 for case (I), ~ 10 for case (II) and a much lower value for case (III). These findings are consistent with experimental observations, such as those from the Pegasus Toroidal Experiment [10], where current amplification factors around 17 were also found to be optimal within a specific operational window, rather than increasing monotonically with injector power.

The sustainment phase is characterized by intermittent relaxation activity, which is crucial for continually feeding current into the plasma core. Upon cessation of the driving flow, configurations that experienced more effective relaxation (cases (I) and (II)) transitioned to a decaying, more axisymmetric state with a slower current decay rate, while the strongly driven case (III) exhibited a rapid current drop due to steep gradients.

In summary, this work provides numerical evidence that LHI via boundary flows is a viable model for solenoid-free startup method for conventional tokamaks like the TCABR upgrade. The success of this approach hinges not on maximizing the helicity injection rate alone, but on optimizing it relative to the confining vertical field to promote beneficial relaxation dynamics that enhance the current multiplication factor. Future work will involve more detailed scans of the parameter space (longer runs in the range of case (I)) and direct quantitative comparisons with experimental data to further refine this startup scenario.

REFERENCES

[1] RAMAN, R. et al., Solenoid-free plasma startup in spherical tokamaks, Plasma Phys. Control. Fusion **56** 103001 (2014).

[2] BONGARD, M. W. et al., Advancing local helicity injection for non-solenoidal tokamak startup, Nucl. Fusion **59** 076003 (2019).

[3] ONO, M. et al., Steady-state tokamak discharge via dc helicity injection, Phys. Rev. Lett. **59** 2165 (1987).

[4] TAYLOR, J. B., Relaxation and magnetic reconnection in plasmas, Rev. Mod. Phys. **58** 741 (1986).

[5] O'BRYAN, J. et al., Simulated flux-rope evolution during non-inductive startup in Pegasus, Plasma Phys. Control. Fusion **56** 064005 (2014).

[6] BOUZAN, A. S. et al., Structural analysis of the in-Vessel RMP IM-Coils of the TCABR tokamak, IEEE Transactions on Plasma Science **52** n. 9 p. 3847 (2024).

[7] GARCIA-MARTINEZ, P. L. et. al., Spheromak formation and sustainment by tangential boundary flows, Phys. Plasmas **17** 050701 (2010).

[8] TOTH, G., General Code for Modeling MHD flows on Parallel Computers: Versatile Advection Code, Astrophys. Lett. Commun. **34** 245 (1996).

[9] BERGER, M. A., Introduction to magnetic helicity, Plasma Phys. Control. Fusion **41** B167 (1999).

[10] BATTAGLIA, D. J. et al., Tokamak startup using outboard current injection on the Pegasus Toroidal Experiment, Nucl. Fusion **51** 073029 (2011).